CHEMISTRY OF MATERIALS
Article

Chem. Mater. **2010,** *22,* 3283–3289 3283
DOI:10.1021/cm100609e

Structural and Chemical Evolution of the SOFC Anode $La_{0.30}Sr_{0.70}Fe_{0.70}Cr_{0.30}O_{3-\delta}$ upon Reduction and Oxidation: An in Situ Neutron Diffraction Study

Jacob M. Haag,[‡] Scott A. Barnett,[§] James W. Richardson, Jr.,[∥] and Kenneth R. Poeppelmeier*[,‡]

[‡]*Department of Chemistry, Northwestern University, Evanston, Illinois 60208,* [§]*Department of Materials Science and Engineering, Northwestern University, Evanston, Illinois 60208, and* [∥]*Intense Pulsed Neutron Source, Argonne National Laboratory, Argonne, Illinois 60439*

Received February 27, 2010. Revised Manuscript Received April 9, 2010

Although some perovskite oxides have been shown to be stable solid oxide fuel cell (SOFC) anodes, the actual crystal structure of these materials under operating conditions is largely unknown. In this paper, the structural evolution of the SOFC anode $La_{0.30}Sr_{0.70}Fe_{0.70}Cr_{0.30}O_{3-\delta}$ was studied at 800 and 900 °C (similar to SOFC operating temperatures) in progressively reducing and oxidizing environments. The perovskite was shown to be stable down to a pO_2 of 10^{-20} atm at 800 °C and a pO_2 of 10^{-18} atm at 900 °C, at which point a spinel phase formed. Further reduction led to the formation of Fe metal. The phase separation of $La_{0.30}Sr_{0.70}Fe_{0.70}Cr_{0.30}O_{3-\delta}$ was also shown to be completely reversible with an increase in the partial oxygen pressure and reoxidation of the sample.

1. Introduction

Solid oxide fuel cells (SOFCs) are electrochemical energy conversion devices that convert chemical energy directly to electrical energy. Currently, cermets such as Ni-$Y_{0.08}Zr_{0.92}O_{2-\delta}$ (YSZ) are commonly used as SOFC anodes because of their excellent electrochemical performance in hydrogen fuel. However, nickel is susceptible to sulfur poisoning and carbon coking, which are detrimental to anode performance.[1,2] To avoid the challenges associated with Ni metal, several groups have studied mixed electron and oxygen ion conducting oxide materials as SOFC anodes. For example, the double perovskite, $Sr_2MgMoO_{6-\delta}$, has shown evidence of sulfur tolerance and yielded a maximum power density of 0.84 W/cm^2 at 800 °C with hydrogen fuel which is comparable to Ni-YSZ anodes.[3,4]

First row transition metal perovskites have also been applied as SOFC anodes but have had limited success since their redox stability is largely dependent on the stability of the transition metal occupying the B-site in the lattice. The relative stability of perovskites follows the general trend: $Cr^{3+} > Fe^{3+} > Mn^{3+} > Co^{3+}$; however, this is the opposite of the trend of the oxygen ion conductivity and oxygen permeability.[5−7] These studies would suggest that for transition metal perovskites to have both good stability and oxide ion conductivity, a combination of cations that are stable to reduction and have good oxide ion mobility can be placed on the B-site of the perovskite.

Recently, several groups have studied $(LaSr)(FeCr)O_{3-\delta}$ solid solutions as SOFC anodes. Tao and Irvine reported that $La_{0.75}Sr_{0.25}Cr_{0.5}Fe_{0.5}O_{3-\delta}$ functions as a stable SOFC anode in H_2 fuel, and it is a complete methane oxidation catalyst.[8] Zhang and Qin studied the perovskite series $La_{0.7}Sr_{0.3}Cr_{1-x}Fe_xO_{3-\delta}$ ($x = 0.2, 0.3, 0.4,$ and 0.5) as potential SOFC anodes and reported that $La_{0.7}Sr_{0.3}Cr_{0.5}Fe_{0.5}O_{3-\delta}$ has the highest conductivity in the series as well as good chemical stability in H_2S.[9] Our group has studied $La_{1/3}Sr_{2/3}Fe_{2/3}Cr_{1/3}O_{3-\delta}$ as a composite anode with $Gd_{0.1}Ce_{0.9}O_{2-\delta}$ (GDC) and shown that it is electrochemically stable in H_2 fuel.[10] The polarization resistance of the $La_{1/3}Sr_{2/3}Fe_{2/3}Cr_{1/3}O_{3-\delta}$-GDC composite is ∼0.25 Ω cm^2 at 800 °C with humidified H_2 as the fuel which is comparable to that of Ni-YSZ anodes, and it is also active toward CO oxidation.[11]

Although perovskite oxides have been shown to be stable SOFC anodes, the actual crystal structure of these materials under operating conditions is largely unknown. In this paper, we performed a detailed in situ neutron diffraction study to gain insight into the structural evolution and stability of the SOFC anode, $La_{0.30}Sr_{0.70}Fe_{0.70}Cr_{0.30}O_{3-\delta}$,

*To whom correspondence should be addressed. E-mail: krp@northwestern.edu.

(1) Matsuzaki, Y.; Yasuda, I. *Solid State Ionics* **2000**, *132*, 261–269.
(2) Finnerty, C. M.; Coe, N. J.; Cunningham, R. H.; Ormerod, R. M. *Catal. Today* **1998**, *46*, 137–145.
(3) Huang, Y. H.; Dass, R. I.; Denyszyn, J. C.; Goodenough, J. B. *J. Electrochem. Soc.* **2006**, *153*, A1266–A1272.
(4) Huang, Y. H.; Dass, R. I.; Xing, Z. L.; Goodenough, J. B. *Science* **2006**, *312*, 254–257.
(5) Nakamura, T.; Petzow, G.; Gauckler, L. J. *Mater. Res. Bull.* **1979**, *14*, 649–659.
(6) Yoo, J.; Verma, A.; Wang, S. Y.; Jacobson, A. J. *J. Electrochem. Soc.* **2005**, *152*, A497–A505.
(7) Konysheva, E.; Irvine, J. T. S. *Chem. Mater.* **2009**, *21*, 1514–1523.
(8) Tao, S. W.; Irvine, J. T. S. *Chem. Mater.* **2004**, *16*, 4116–4121.
(9) Zhang, X. Z. *Qin Huagong Jinzhan* **2009**, *28*, 788–792.
(10) Haag, J. M.; Madsen, B. D.; Barnett, S. A.; Poeppelmeier, K. R. *Electrochem. Solid-State Lett.* **2008**, *11*, B51–B53.
(11) Bierschenk, D. M.; Haag, J. M.; Poeppelmeier, K. R.; Barnett, S. A. In *SOFC XI*, Vienna, 2009; Vol. ECS Transactions, pp 2107−2116.

© 2010 American Chemical Society
Published on Web 04/26/2010

under reducing and oxidizing conditions, similar to SOFC anode operating conditions. The stability limit of $La_{0.30}Sr_{0.70}Fe_{0.70}Cr_{0.30}O_{3-\delta}$ and the phase separation products were determined. Phase separation was also shown to be reversible with an increase in the partial oxygen pressure and reoxidation of the sample. The results of this study have direct implications for the application of $La_{0.30}Sr_{0.70}Fe_{0.70}Cr_{0.30}O_{3-\delta}$ as a SOFC anode.

2. Experimental Section

2.1. Synthesis and Sample Preparation. A sample with the nominal composition $La_{1/3}Sr_{2/3}Fe_{2/3}Cr_{1/3}O_{3-\delta}$ was synthesized by traditional solid state reaction. La_2O_3 was precalcined at 800 °C to remove all hydroxides, ground together with Fe_2O_3, Cr_2O_3, and $SrCO_3$, and fired at 1250 °C for 24 h with intermittent grindings. The $La_{1/3}Sr_{2/3}Fe_{2/3}Cr_{1/3}O_{3-\delta}$ sample was then isostatically pressed into a rod, sintered at 1300 °C for 6 h in air, and cooled to room temperature for the neutron powder diffraction experiment.

2.2. Powder X-ray Diffraction. Powder X-ray diffraction was performed using a Scintag XDS 2000 diffractometer with Cu Kα radiation and a nickel filter. Patterns were collected at room temperature in air in the $15° < 2\delta < 80°$ range with a 0.02° step size and a 1 s dwell time.

2.3. Neutron Diffraction. Time-of-flight neutron diffraction data were collected on the General Purpose Powder Diffractometer (GPPD) at the Intense Pulsed Neutron Source at Argonne National Laboratory. The $La_{1/3}Sr_{2/3}Fe_{2/3}Cr_{1/3}O_{3-\delta}$ sample was mounted in a "Miller" furnace and heated to 800 °C in air. At 800 °C, $La_{1/3}Sr_{2/3}Fe_{2/3}Cr_{1/3}O_{3-\delta}$ was reduced and reoxidized using a combination of different gas mixtures. $La_{1/3}Sr_{2/3}Fe_{2/3}Cr_{1/3}O_{3-\delta}$ was then heated to 900 °C in air, reduced, and cooled to room temperature under flowing Ar. The oxygen partial pressures were adjusted using gas mixtures of air, Ar, CO_2, 1% CO/Ar, and CO. The gas flows were controlled with Brooks Series 5820 mass flow controllers. The pO_2 was monitored by a solid zirconia electrolyte oxygen sensor (Ceramic Oxide Fabricators SIRO2). The pO_2 values were calculated by the "NASA computer program for the calculation of chemical equilibriums".[12] All of the diffraction data were collected in the $2\theta = \pm 90°$ detector banks and analyzed using Rietveld[13] profile analysis with GSAS and EXPGUI.[14,15]

A complete refinement was performed at room temperature in air, which included lattice parameters, thermal parameters, atom occupancies, peak shape coefficients, absorption coefficients, and phase fractions. During the progressive reduction and oxidation, data were collected at 15 min intervals for 6 h for each gas mixture. The lattice parameters, peak shape coefficients, thermal coefficients, and oxygen occupancy of each pattern were sequentially refined. This allowed the change in lattice constant and oxygen occupancy to be monitored in situ at 15 min intervals. The statistics for the 15 min scans were limited; therefore, when the lattice parameters stabilized (< 0.002 Å change) in each gas mixture, the data were merged and a more complete refinement was performed. This allowed the stability limit and phase separation products to be determined.

2.4. Elemental Analysis. The cation ratios were determined by inductively coupled plasma atomic emission spectroscopy (ICP-AES) using a Thermo Jarrell Ash Atomscan model 25 sequential ICP spectrometer equipped with vacuum optics covering the spectral range from 160 to 850 nm. The sample was dissolved hydrothermally using a Parr pressure vessel in aqua regia at 100 °C for 6 h and then diluted to the appropriate concentrations with deionized water. Three measurements were taken per sample and averaged which gave a La:Sr:Fe:Cr cation ratio of 0.334:0.666:0.666:0.334.

2.5. Differential Thermal Analysis. Differential thermal analysis (DTA) was performed on a Shimadzu DTA-50 differential thermal analyzer. Measurements were taken in a static air atmosphere using platinum crucibles and an alumina powder reference. The heating profile consisted of a 5 °C/min linear ramp from ambient temperature to 900 °C.

2.6. Thermal Gravimetric Analysis. Thermogravimetric analysis (TGA) was performed on a TA Q50 thermogravimetric analyzer (TA Instruments) under dry N_2 (80 mL/min). The sample was heated from ambient temperature to 800 °C at a rate of 1 °C/min and held at 800 °C for 6 h.

3. Results and Discussion

3.1. Room-Temperature Neutron Diffraction. Figure 1 shows the room-temperature neutron diffraction pattern of the as-prepared sample with the nominal stoichiometry $La_{1/3}Sr_{2/3}Fe_{2/3}Cr_{1/3}O_{3-\delta}$. The sample exhibits a pseudocubic rhombohedral structure and was initially refined in space group $R\bar{3}c$ (167) as a single phase (Figure 1a). The $R\bar{3}c$ model fit all of the peaks in the neutron diffraction pattern except for a shoulder at ~2.225 Å. Since the shoulder could not be indexed in the $R\bar{3}c$ space group, lower-symmetry perovskites were modeled. The lowering of the symmetry did not fit the shoulder which suggested the presence of a second phase. Two phase refinements were then performed, and several different phases were modeled. The best fit occurred when $LaCrO_3$ was fit to orthorhombic space group *Pnma* (62) as the second phase (Figure 1b). The shoulder lines up directly with the (220) peak in $LaCrO_3$ *Pnma* and significantly improved the χ^2 and R values of the refinement.

The identification of $LaCrO_3$ indicates that the major perovskite phase is not actually $La_{1/3}Sr_{2/3}Fe_{2/3}Cr_{1/3}O_{3-\delta}$, but instead a more Sr and Fe rich phase. To quantify the cation stoichiometry in the major perovskite phase, the phase fractions and cation occupancies were refined. The phase fractions were refined without constraints, while the occupancies of the A- and B-sites of the perovskite were each fixed at 1. At the same time, because the second phase is $LaCrO_3$, the occupancies of Sr and Fe in the structure were constrained together and were oppositely constrained to La and Cr (i.e., $La_{0.334-x}Sr_{0.666+x}Fe_{0.666+x}Cr_{0.334-x}O_{3-\delta}$). The refined phase fractions and cation occupancies gave similar results. The refined cation occupancies gave the approximate chemical formula $La_{0.30}Sr_{0.70}Fe_{0.70}Cr_{0.30}O_3$ for the major perovskite phase. Similarly, the refined phase fractions gave mole percentages of 95.1% $La_{0.30}Sr_{0.70}Fe_{0.70}Cr_{0.30}O_3$ and 4.9% $LaCrO_3$, which can be used to calculate the cation stoichiometry of the major perovskite phase, $La_{0.30}Sr_{0.70}Fe_{0.70}Cr_{0.30}O_3$. Therefore,

(12) McBride, B. J.; Gordon, S. In NASA Refernce Publication 1311, **1996**.
(13) Rietveld, H. M. *J. Appl. Crystallogr.* **1969**, *2*, 65.
(14) Larson, A. C.; Von Dreele, R. B. *General Structure Analysis System* (*GSAS*), Los Alamos National Laborartory Report LAUR 86-748; Los Alamos National Laboratory: Los Alamos, NM, 1994.
(15) Toby, B. H. *J. Appl. Crystallogr.* **2001**, *34*, 210–213.

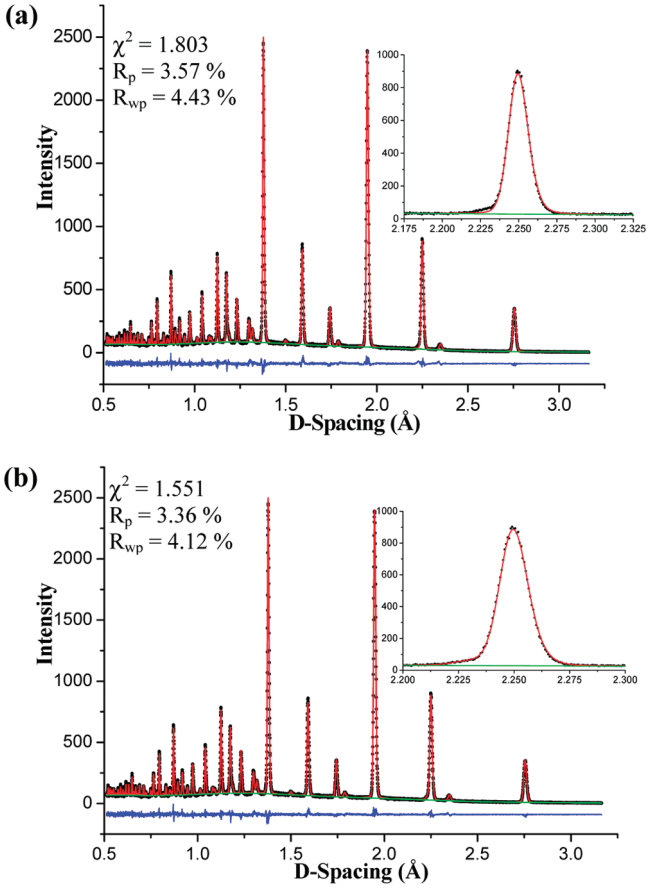

Figure 1. Observed (dots), calculated (red line), background (green line), and difference (blue line) profiles for the room-temperature neutron diffraction of $La_{1/3}Sr_{2/3}Fe_{2/3}Cr_{1/3}O_{3-\delta}$. Panel a is a single-phase ($R\bar{3}c$) refinement, and panel b is a two-phase ($R\bar{3}c$ and *Pnma*) refinement. The inset is a magnification of the shoulder at ~2.225 Å.

Table 1. Room-Temperature Structural Parameters of the $La_{1/3}Sr_{2/3}Fe_{2/3}Cr_{1/3}O_{3-\delta}$ Sample Obtained from Neutron Diffraction Data[a]

atom	site	occupancy	*x*	*y*	*z*	U_{iso} (×100 Å^2)
		$La_{0.334-x}Sr_{0.666+x}Fe_{0.666+x}Cr_{0.334-x}O_{3-\delta}$, $R\bar{3}c$[b]				
La	6a	0.29(9)	0	0	0.25	1.02(2)
Sr	6a	0.70(1)	0	0	0.25	1.02(2)
Fe	6b	0.70(1)	0	0	0	0.46(0)
Cr	6b	0.29(9)	0	0	0	0.46(0)
O	18e	1.00(1)	0.521(1)	0	0	1.68(5)
		$LaCrO_3$, Minor Perovskite Phase, *Pnma*[c]				
La	4c	1.00	0.019(6)	0.25	−0.004(6)	2.50(0)
Cr	4b	1.00	0	0	0.5	2.50(0)
O	4c	1.00	0.4935	0.25	0.067(6)	2.50(0)
O	8d	1.00	0.226(5)	0.533(8)	0.226(5)	2.50(0)

[a] χ^2 = 1.551. R_p = 3.36%. R_{wp} = 4.12%. [b] Space group $R\bar{3}c$ (167). sa = 5.5069(5) Å, and *c* = 13.4671(9) Å. Mole percent = 95.1%. [c] Space group *Pnma* (62). *a* = 5.4892(3) Å, *b* = 7.6474(3) Å, and *c* = 5.5678(3) Å. Mole percent = 4.9%.

the cation occupancies were fixed at $La_{0.30}Sr_{0.70}Fe_{0.70}Cr_{0.30}O_{3-\delta}$, and the fraction of $LaCrO_3$ was fixed at 4.9% for the high-temperature experiment. Table 1 includes the details of the room-temperature neutron powder diffraction refinement, including the refined cation occupancies and the refined phase fractions.

Previously, Kozhevnikov et al. reported an X-ray powder diffraction study of $La_{1/3}Sr_{2/3}Fe_{2/3}Cr_{1/3}O_{3-\delta}$ in which

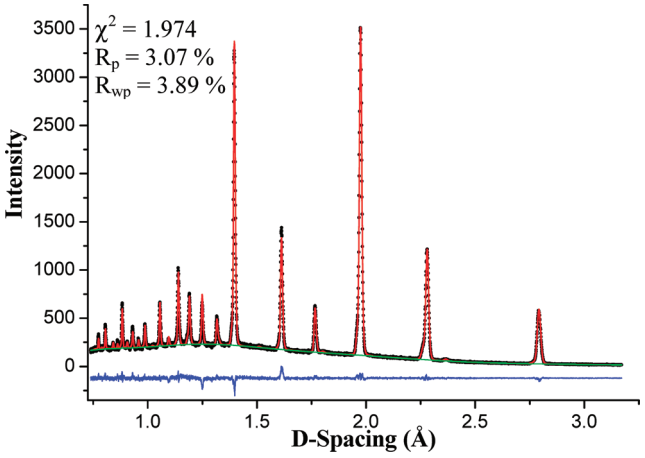

Figure 2. Observed (dots), calculated (red line), background (green line), and difference (blue line) profiles for the neutron diffraction of $La_{0.30}Sr_{0.70}Fe_{0.70}Cr_{0.30}O_{3-\delta}$ and $LaCrO_3$ at 800 °C in air.

Table 2. Structural Parameters of $La_{0.30}Sr_{0.70}Fe_{0.70}Cr_{0.30}O_{3-\delta}$ and $LaCrO_3$ at 800 °C in Air Obtained from Neutron Diffraction Data[a]

atom	site	occupancy	*x*	*y*	*z*	U_{iso} (×100 Å^2)
		$La_{0.30}Sr_{0.70}Fe_{0.70}Cr_{0.30}O_{3-\delta}$, $Pm\bar{3}m$[b]				
La	1a	0.30	0	0	0	3.33(2)
Sr	1a	0.70	0	0	0	3.33(2)
Fe	1b	0.70	0.5	0.5	0.5	2.29(7)
Cr	1b	0.30	0.5	0.5	0.5	2.29(7)
O	3c		0	0.5	0.5	4.57(1)
		$LaCrO_3$, $R\bar{3}c$[c]				
La	6a	1.00	0	0	0.25	1.70(9)
Cr	6b	1.00	0	0	0	0.92(6)
O	18e	1.00	0.459(7)	0	0.25	2.55(2)

[a] χ^2 = 1.974. R_p = 3.07%. R_{wp} = 3.89%. [b] Space group $Pm\bar{3}m$ (221). *a* = 3.9446(2) Å. [c] Space group *Pnma* (167). *a* = 5.5475(8) Å, and *c* = 13.5190(8) Å.

the perovskite was indexed to space group $R\bar{3}c$ with the following unit cell dimensions: *a* = 5.5094(5) Å, and *c* = 13.4476(8) Å.[16] They also reported the presence of trace amounts of $SrCrO_4$, which diffused into the perovskite structure upon reduction. No $SrCrO_4$ was observed in our experiment; however, the presence of low concentrations of second phases in both Kozhevnikov's experiment ($SrCrO_4$) and ours ($LaCrO_3$) suggests that the solubility limit of Cr in $La_{1/3}Sr_{2/3}Fe_{1-x}Cr_xO_{3-\delta}$ is ~$^1/_3$. We verified this by attempting to synthesize samples with a fixed La:Sr ratio of 1:2 while increasing the concentration of Cr at the B-site. Samples with the nominal stoichiometries $La_{0.333}Sr_{0.667}Fe_{0.60}Cr_{0.40}O_{3-\delta}$, $La_{0.333}Sr_{0.667}Fe_{0.50}Cr_{0.50}O_{3-\delta}$, and $La_{0.333}Sr_{0.667}Fe_{0.25}Cr_{0.75}O_{3-\delta}$ showed increasing amounts of $SrCrO_4$ with an increasing Cr concentration (see Figure S1 of the Supporting Information).

3.2. Structure from Room Temperature to 800 °C. The sample containing both $La_{0.30}Sr_{0.70}Fe_{0.70}Cr_{0.30}O_{3-\delta}$ and $LaCrO_3$ was heated to 800 °C in air. Figure 2 shows the 800 °C neutron powder diffraction pattern of the

(16) Kozhevnikov, V. L.; Leonidov, I. A.; Bahteeva, J. A.; Patrakeev, M. V.; Mitberg, E. B.; Poeppelmeier, K. R. *Chem. Mater.* **2004**, *16*, 5014–5020.

two-phase sample. $La_{0.30}Sr_{0.70}Fe_{0.70}Cr_{0.30}O_{3-\delta}$ was indexed and refined to cubic space group $Pm\bar{3}m$ (221) with a lattice constant of 3.9446(2) Å. Heating from room temperature to 800 °C causes $La_{0.30}Sr_{0.70}Fe_{0.70}Cr_{0.30}O_{3-\delta}$ to undergo a phase transition from a rhombohedral structure to a cubic structure. $LaCrO_3$ was still present and refined to space group $R\bar{3}c$, which is consistent with previous studies showing that $LaCrO_3$ undergoes a phase transition at 260 °C from orthorhombic to rhombohedral.[17] Table 2 includes the details of the 800 °C neutron powder diffraction refinement in air.

DTA was also performed to determine the temperature at which the $R\bar{3}c$ to $Pm\bar{3}m$ phase transition of $La_{0.30}Sr_{0.70}Fe_{0.70}Cr_{0.30}O_{3-\delta}$ occurs; however, the experiment was inconclusive. The enthalpy of $La_{0.30}Sr_{0.70}Fe_{0.70}Cr_{0.30}O_{3-\delta}$ was continuous through the phase transition, and neither an endothermic nor an exothermic peak was observed (Figure S2 of the Supporting Information). This demonstrates that the rhombohedral-to-cubic phase transition is a second-order phase transition. Similar observations have been reported for the rhombohedral-to-cubic phase transition in $La_{0.7}Sr_{0.3}FeO_{3-\delta}$, $La_{0.6}Sr_{0.4}FeO_{3-\delta}$, and $La_{0.5}Sr_{0.5}FeO_{3-\delta}$.[18]

3.3. General Trend of Reduction and/or Oxidation of $La_{0.30}Sr_{0.70}Fe_{0.70}Cr_{0.30}O_{3-\delta}$ at 800 °C. To study the structural evolution of $La_{0.30}Sr_{0.70}Fe_{0.70}Cr_{0.30}O_{3-\delta}$ under highly reducing and oxidizing conditions at 800 °C, we subjected the sample to various partial oxygen pressures. The structure remained cubic perovskite during both the reduction and oxidation, and the stability limit was determined to be at a pO_2 of 10^{-20} atm.

Figure 3 shows the change in lattice constant of $La_{0.30}Sr_{0.70}Fe_{0.70}Cr_{0.30}O_{3-\delta}$ and the corresponding measured partial oxygen pressure plotted versus time. Each point in Figure 3 represents an individually refined neutron diffraction pattern that was collected for 15 min. The lattice constant increased with a decreasing pO_2, which is caused by the increase in oxygen vacancies and the reduction of the B-site cation to maintain charge balance. The ionic radii of Fe and Cr increase when they are reduced from an oxidation state of +4 [$r_{VI}(Fe^{4+}) = 0.585$, and $r_{VI}(Cr^{4+}) = 0.55$ Å] to +3 [$r_{VI}(Fe^{3+}) = 0.645$ Å, and $r_{VI}(Cr^{3+}) = 0.615$ Å].[19] Figure 4 shows the chemical linear expansion of $La_{0.30}Sr_{0.70}Fe_{0.70}Cr_{0.30}O_{3-\delta}$. Since the lattice constant of $La_{0.30}Sr_{0.70}Fe_{0.70}Cr_{0.30}O_{3-\delta}$ increases upon reduction, the linear expansion of $La_{0.30}Sr_{0.70}Fe_{0.70}Cr_{0.30}O_{3-\delta}$ was calculated to determine the magnitude of the expansion. The change in the lattice constant was $< 0.28\%$ at 800 °C during the reduction (prior to phase separation). Also, the change in volume of $LaCrO_3$ during reduction and oxidation was significantly smaller than that of $La_{0.30}Sr_{0.70}Fe_{0.70}Cr_{0.30}O_{3-\delta}$ since Cr^{3+} is less susceptible to reduction than Fe^{4+} and Cr^{4+} and oxygen vacancies are less likely to form.

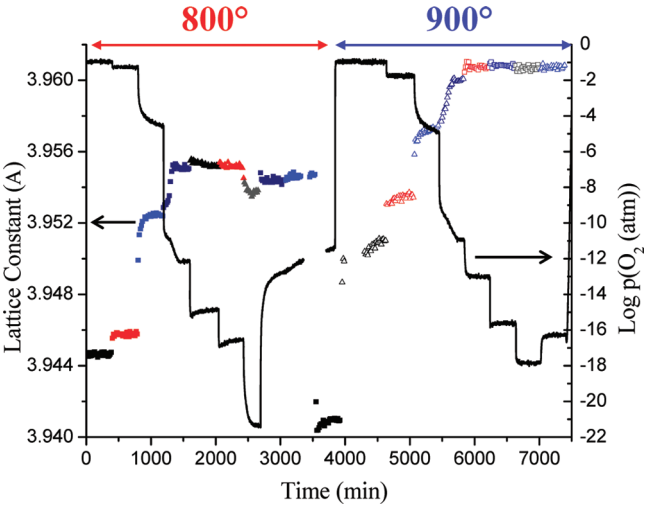

Figure 3. Change in the lattice constant of $La_{0.30}Sr_{0.70}Fe_{0.70}Cr_{0.30}O_{3-\delta}$ and corresponding measured partial oxygen pressure plotted vs time. The change in the lattice constant of $La_{0.30}Sr_{0.70}Fe_{0.70}Cr_{0.30}O_{3-\delta}$ is depicted by 420 neutron diffraction patterns. Each point represents an individually refined diffraction pattern, and the color changes represent changes in gas composition.

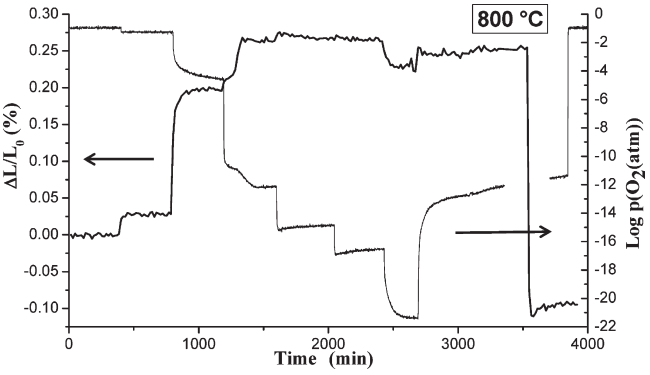

Figure 4. Chemical linear expansion of $La_{0.30}Sr_{0.70}Fe_{0.70}Cr_{0.30}O_{3-\delta}$ and corresponding measured partial oxygen pressure plotted vs time at 800 °C. L_0 is the initial lattice constant at 800 °C in air.

The lattice constant and volume of $La_{0.30}Sr_{0.70}Fe_{0.70}Cr_{0.30}O_{3-\delta}$ increased until the pO_2 dropped below 10^{-20} atm. At this point, the major perovskite phase, $La_{0.30}Sr_{0.70}Fe_{0.70}Cr_{0.30}O_{3-\delta}$, began evolving into multiple phases. A third phase was observed and refined to the cubic spinel structure, space group $Fd\bar{3}m$ (227) (Figure 5). A further decrease in pO_2 ($< 10^{-21.5}$ atm) led to an increase in the concentration of the spinel phase and the formation of α-Fe [$Im\bar{3}m$ (229)] (Figure 6).

The identification of the phase separation products indicated that $La_{0.30}Sr_{0.70}Fe_{0.70}Cr_{0.30}O_{3-\delta}$ had been reduced beyond its stability limit at 800 °C; therefore, the sample was reoxidized. Increasing the pO_2 from $10^{-21.5}$ to 10^{-14} atm caused the concentration of the spinel and α-Fe to decrease. Increasing the pO_2 to $> 10^{-13}$ atm caused α-Fe to diffuse completely back into the oxide structures, and three phases, $LaCrO_3$, "$La_{0.3}Sr_{0.7}Fe_{0.70}Cr_{0.30}O_{3-\delta}$", and the spinel, remained. As the pO_2 increased, the volume of $La_{0.30}Sr_{0.70}Fe_{0.70}Cr_{0.30}O_{3-\delta}$ decreased, which is consistent with the decrease in oxygen vacancies and the reoxidation of the B-site from the +3 state to the +4 state.

(17) Oikawa, K.; Kamiyama, T.; Hashimoto, T.; Shimojyo, Y.; Morii, Y. *J. Solid State Chem.* **2000**, *154*, 524–529.
(18) Fossdal, A.; Menon, M.; Waernhus, I.; Wiik, K.; Einarsrud, M. A.; Grande, T. *J. Am. Ceram. Soc.* **2004**, *87*, 1952–1958.
(19) Shannon, R. D.; Prewitt, C. T. *Acta Crystallogr.* **1969**, *B25*, 925.

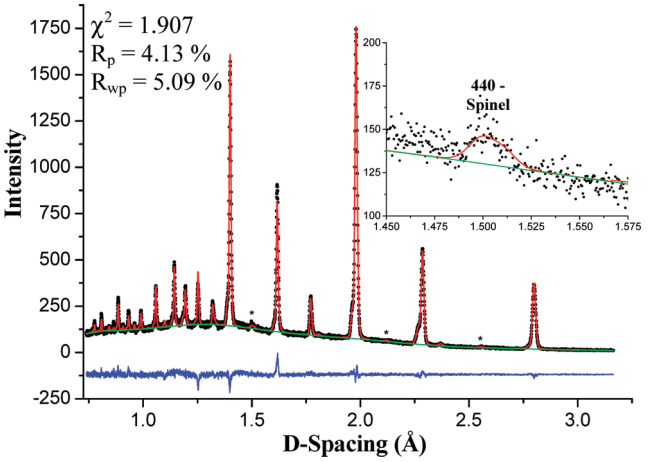

Figure 5. Observed (dots), calculated (red line), background (green line), and difference (blue line) profiles for the neutron diffraction of $La_{0.30}Sr_{0.70}Fe_{0.70}Cr_{0.30}O_{3-\delta}$, $LaCrO_3$, and spinel at 800 °C and a pO_2 of 10^{-20} atm. The spinel phase ($Fd\bar{3}m$) is marked with an asterisk. The inset is a magnification of the 440 peak of the spinel phase.

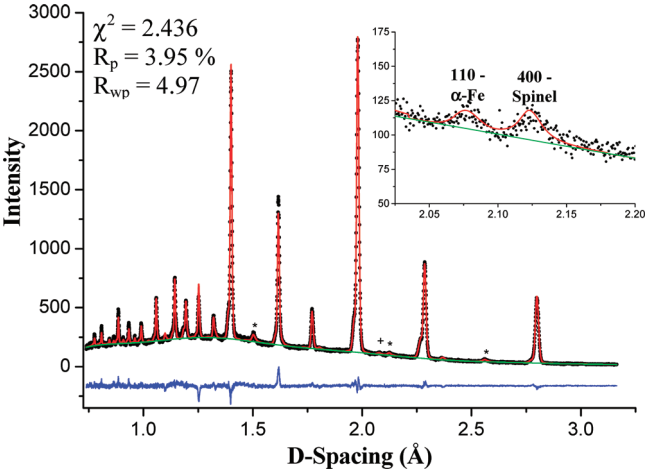

Figure 6. Observed (dots), calculated (red line), background (green line), and difference (blue line) profiles for the neutron diffraction of $La_{0.30}Sr_{0.70}Fe_{0.70}Cr_{0.30}O_{3-\delta}$, $LaCrO_3$, spinel, and α-Fe at 800 °C and a pO_2 of $10^{-21.5}$ atm. The spinel ($Fd\bar{3}m$) (∗) and α-Fe (+) phases are marked. The inset is a magnification of the 110 peak of α-Fe and the 400 peak of the spinel.

The volume of $La_{0.30}Sr_{0.70}Fe_{0.70}Cr_{0.30}O_{3-\delta}$ at 800 °C in air was smaller after reoxidation because the perovskite remained slightly B-site deficient with trace amounts of spinel still present.

Although it was not possible to determine the exact composition of the spinel phase, it can be assumed that the A-site of the spinel is Fe^{2+} since Fe^{3+} is less stable to reduction than Cr^{3+}. The B-site of the spinel is more difficult to identify; however, since Fe and Cr are disordered in the perovskite structure, it is likely that the spinel is a solid solution [$Fe(Fe_{2-x}Cr_x)O_4$] with a mixture of Fe^{3+} and Cr^{3+}on the B-site. The presence of the spinel phase at a pO_2 of $10^{-21.5}$ atm is also further evidence that the composition is $Fe(Fe_{2-x}Cr_x)O_4$. If the spinel phase did not contain Cr, then it would be expected to undergo a phase transition to the face-centered cubic structure FeO [$Fm\bar{3}m$ (225)].[20] However, on the basis of the Fe-Cr-pO_2 phase diagram reported by Mikkelsen and Linderoth, the solid solution, $Fe(Fe_{2-x}Cr_x)O_4$, and α-Fe form an equilibrium at a pO_2 of $\sim 10^{-21}$ atm,[21] which is consistent with our observations.

It should also be pointed out that there were no additional strontium- and lanthanum-containing phases during the reduction. Further reduction would have likely led to further decomposition of $La_{0.30}Sr_{0.70}Fe_{0.70}Cr_{0.30}O_{3-\delta}$. However, at 800 °C and a corresponding pO_2 of $10^{-21.5}$ atm, $La_{0.30}Sr_{0.70}Fe_{0.70}Cr_{0.30}O_{3-\delta}$ becomes B-site deficient but the cubic perovskite structure remains intact. There was also no evidence of decomposition of $LaCrO_3$, which is consistent with the results of Staoh et al.,[22] who reported that $LaCrO_3$ is stable to pO_2 value of $< 10^{-24}$ atm.

3.4. General Trend of Reduction and/or Oxidation of $La_{0.30}Sr_{0.70}Fe_{0.70}Cr_{0.30}O_{3-\delta}$ at 900 °C. The mixture containing "$La_{0.30}Sr_{0.70}Fe_{0.70}Cr_{0.30}O_{3-\delta}$", spinel, and $LaCrO_3$ was heated from 800 to 900 °C in air. Heating to 900 °C caused the spinel to diffuse back into the major perovskite phase, returning the stoichiometry to $La_{0.30}Sr_{0.70}Fe_{0.70}Cr_{0.30}O_{3-\delta}$. Similar to the reduction at 800 °C, the volume of $La_{0.30}Sr_{0.70}Fe_{0.70}Cr_{0.30}O_{3-\delta}$ increased with a decreasing pO_2 as oxygen vacancies were created in the lattice and the B-site cations were reduced (Figure 3). The chemical linear expansion was calculated at 900 °C and found to be <0.28% (Figure S3 of the Supporting Information). At a pO_2 of 10^{-18} atm, a trace amount of spinel could be observed, indicating the stability limit of $La_{0.30}Sr_{0.70}Fe_{0.70}Cr_{0.30}O_{3-\delta}$ had been reached at 900 °C. The pO_2 was increased to $10^{-16.5}$ atm which caused the spinel to diffuse back into the perovskite structure. The sample was then cooled to room temperature under argon.

3.5. Oxygen Stoichiometry of $La_{0.30}Sr_{0.70}Fe_{0.70}Cr_{0.30}O_{3-\delta}$. Figure 7 displays the refined oxygen stoichiometry of $La_{0.30}Sr_{0.70}Fe_{0.70}Cr_{0.30}O_{3-\delta}$ and the corresponding measured partial oxygen pressures plotted versus time. The oxygen stoichiometry closely tracks the measured pO_2 which is consistent with a well-mixed gas phase and a sample with an oxygen activity that is in near equilibrium with the gas. A TGA experiment was also performed to verify the accuracy of the refined oxygen stoichiometry. Figure 8 shows the thermal gravimetric curve of the oxygen stoichiometry and temperature versus time under flowing N_2. The points on the graph represent the refined oxygen occupancies at 800 °C under argon from the neutron experiment. As one can see from the graph, the results from the TGA experiment are in very good agreement with the refined oxygen stoichiometry from the neutron experiment. Both experiments demonstrate that the oxygen stoichiometry for $La_{0.30}Sr_{0.70}Fe_{0.70}Cr_{0.30}O_{3-\delta}$ is ~2.82 at 800 °C in argon.

During the neutron experiment (Figure 6), the oxygen stoichiometry stabilized at approximately ~2.65 at 800 °C before $La_{0.30}Sr_{0.70}Fe_{0.70}Cr_{0.30}O_{3-\delta}$ was reduced beyond the stability limit, which is consistent with the B-site of

(20) Muan, A. *Am. J. Sci.* **1958**, *256*, 171–207.

(21) Mikkelsen, L.; Linderoth, S. *Mater. Sci. Eng., A* **2003**, *361*, 198–212.

(22) Satoh, H.; Koseki, S.; Takagi, M.; Chung, W. Y.; Kamegashira, N. *J. Alloys Compd.* **1997**, *259*, 176–182.

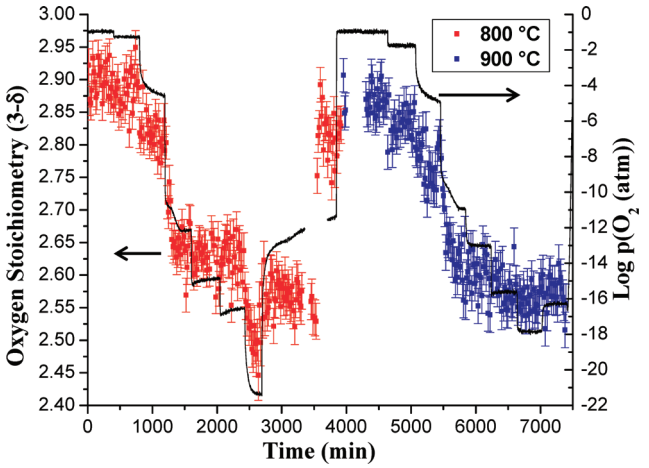

Figure 7. Refined oxygen stoichiometry of $La_{0.30}Sr_{0.70}Fe_{0.70}Cr_{0.30}O_{3-\delta}$ and corresponding measured partial oxygen pressures plotted vs time. The oxygen stoichiometry is represented by 420 individually refined neutron diffraction patterns. Each point represents the refined oxygen stoichiometry from an individual neutron diffraction pattern.

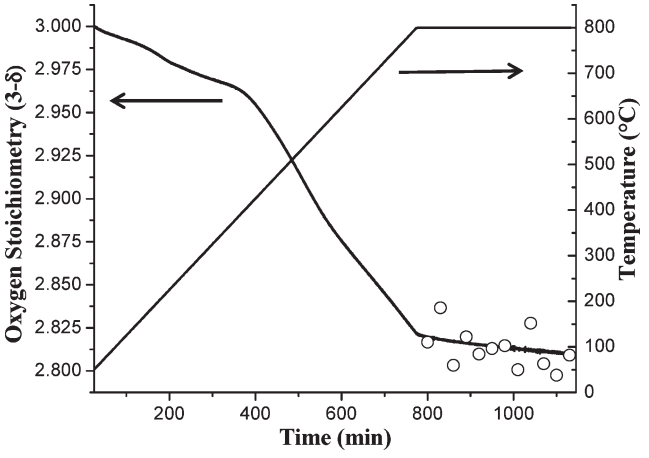

Figure 8. TGA curve of the oxygen stoichiometry under flowing N_2 and temperature plotted vs time. The points on the graph represent the refined oxygen occupancies at 800 °C under argon from the neutron diffraction experiment.

$La_{0.30}Sr_{0.70}Fe_{0.70}Cr_{0.30}O_{3-\delta}$ being fully reduced to the +3 state. Although a large number of oxygen vacancies were formed ($\delta = 0.35$) in $La_{0.30}Sr_{0.70}Fe_{0.70}Cr_{0.30}O_{\sim 2.65}$, it retained the cubic perovskite structure and the vacancies were disordered. In the parent compound, $La_{0.30}Sr_{0.70}FeO_{\sim 2.65}$, the oxygen vacancies order into an orthorhombic triple perovskite with repeating octahedral−octahedral−tetrahedral layers.[23] The disordering of the oxygen vacancies in the chromium-substituted analogue can be explained by the low concentration of Cr on the B-site. Assuming the B-site cations are fully disordered, statistically two-thirds of the Cr atoms are in what would be the octahedral layers of the pure iron compound, while one-third of the atoms are present in what would be the tetrahedral layer. Chromium has a higher affinity for 6-fold coordination than Fe when it is placed on a tetrahedral site; it

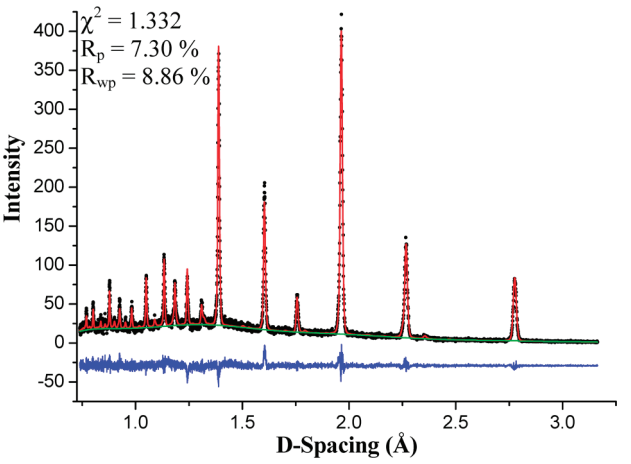

Figure 9. Observed (dots), calculated (red line), background (green line), and difference (blue line) profiles for the neutron diffraction of $La_{0.30}Sr_{0.70}Fe_{0.70}Cr_{0.30}O_{3-\delta}$ and $LaCrO_3$ after they had been cooled from 900 °C to room temperature under flowing argon.

disrupts the tetrahedral layer by drawing oxygen ions from two surrounding Fe octahedra, thus transforming two iron octahedra (FeO_3) to pyramids ($FeO_{2.5}$). At the same time, the two oxygen ions, which are now coordinated with Cr forming an octahedron in the "tetrahedral layer", also coordinate with two iron tetrahedra (FeO_2), transforming them into pyramids ($FeO_{2.5}$).[16] Therefore, the placement of one chromium atom on a tetrahedral site directly affects the coordination of five polyhedra. The chromium atoms are randomly distributed, which transforms the ordered orthorhombic structure of $La_{0.30}Sr_{0.70}FeO_{2.65}$ to the disordered cubic structure of $La_{0.30}Sr_{0.70}Fe_{0.70}Cr_{0.30}O_{2.65}$.

Although it could be argued that the oxygen vacancies are thermally disordered, this is highly unlikely. Leonidov et al.[24] reported that the vacancy-ordered triple perovskite structure of $La_{0.30}Sr_{0.70}FeO_{3-\delta}$ is stable between 750 and 950 °C at low partial oxygen pressures. Therefore, if $La_{0.30}Sr_{0.70}Fe_{0.70}Cr_{0.30}O_{2.65}$ did order, we would anticipate high-temperature vacancy ordering and stability similar to those of the parent iron compound which did not occur.

After the 900 °C in situ neutron diffraction experiment, the sample was cooled to room temperature under flowing argon to determine if the vacancies would order upon cooling. $La_{0.30}Sr_{0.70}Fe_{0.70}Cr_{0.30}O_{3-\delta}$ retained the cubic structure, $Pm\bar{3}m$, and the vacancies remained disordered (Figure 9). The oxygen occupancy was refined at room temperature and determined to be ~2.65 (similar to the high-temperature results). Table 3 includes the details of the postreduction room-temperature neutron powder diffraction refinement.

4. Conclusion

A detailed in situ neutron diffraction study was performed to gain insight into the structural evolution and stability of the SOFC anode, $La_{0.30}Sr_{0.70}Fe_{0.70}Cr_{0.30}O_{3-\delta}$,

(23) Battle, P. D.; Gibb, T. C.; Lightfoot, P. *J. Solid State Chem.* **1990**, *84*, 237–244.

(24) Leonidov, I. A.; Kozhevnikov, V. L.; Patrakeev, M. V.; Mitberg, E. B.; Poeppelmeier, K. R. *Solid State Ionics* **2001**, *144*, 361–369.

Table 3. Structural Parameters of $La_{0.30}Sr_{0.70}Fe_{0.70}Cr_{0.30}O_{3-\delta}$ and $LaCrO_3$ after They Had Been Cooled from 900 °C to Room Temperature under Flowing Argon[a]

atom	site	occupancy	x	y	z	U_{iso} ($\times 100$ Å^2)
			$La_{0.30}Sr_{0.70}Fe_{0.70}Cr_{0.30}O_{3-\delta}$, $Pm\bar{3}m$[b]			
La	1a	0.30	0	0	0	3.18(8)
Sr	1a	0.70	0	0	0	3.18(8)
Fe	1b	0.70	0.5	0.5	0.5	2.27(6)
Cr	1b	0.30	0.5	0.5	0.5	2.27(6)
O	3c	0.88(2)	0	0.5	0.5	4.56(0)
			$LaCrO_3$, $R\bar{3}c$[c]			
La	6a	1.00	0.019(6)	0.25	−0.004(6)	0.97(1)
Cr	6b	1.00	0	0	0.5	0.71(2)
O	18e	1.00	0.493(5)	0.25	0.067(6)	5.43(0)
O	8d	1.00	0.226(5)	0.533(8)	0.226(5)	1.31(5)

[a] $\chi^2 = 1.332$. $R_p = 7.30\%$. $R_{wp} = 8.86\%$. [b] Space group $Pm\bar{3}m$ (221). $a = 3.9217(1)$ Å. [c] Space group $R\bar{3}c$ (167). $a = 5.5045(5)$ Å, $b = 7.6935(8)$ Å, and $c = 5.5474(6)$ Å.

under reducing and oxidizing conditions at 800 and 900 °C. At room temperature, $La_{0.30}Sr_{0.70}Fe_{0.70}Cr_{0.30}O_{3-\delta}$ exhibits a rhombohedral structure, in space group $R\bar{3}c$. When $La_{0.30}Sr_{0.70}Fe_{0.70}Cr_{0.30}O_{3-\delta}$ is heated to 800 °C in air, it undergoes a second-order phase transition to a cubic structure, in space group $Pm\bar{3}m$. The second-order phase transition of $La_{0.30}Sr_{0.70}Fe_{0.70}Cr_{0.30}O_{3-\delta}$ is favorable for SOFC fabrication to prevent delamination of the anode and electrolyte which can be caused by abrupt phase transitions and rapid volume changes.[25] $La_{0.30}Sr_{0.70}Fe_{0.70}Cr_{0.30}O_{3-\delta}$ was then reduced at 800 and 900 °C and remained cubic even though a large number of oxygen vacancies were formed ($\delta \leq 0.35$). This is advantageous for a SOFC anode because it minimizes the stresses caused by redox cycling. Also, the change in the linear expansion of $La_{0.30}Sr_{0.70}Fe_{0.70}Cr_{0.30}O_{3-\delta}$ during reduction was relatively small (< 0.28%) at 800 and 900 °C, which is important because mechanical modeling has shown that active anode layers in SOFCs require a linear expansion of < 1%; otherwise, delamination at the anode−electrolyte interface is likely to occur.[26,27]

(25) Tao, S. W.; Irvine, J. T. S. *Chem. Mater.* **2006**, *18*, 5453–5460.
(26) Sarantaridis, D.; Atkinson, A. *Fuel Cells* **2007**, *7*, 246–258.
(27) Fu, Q. X.; Tietz, F. *Fuel Cells* **2008**, *8*, 283–293.

The perovskite, $La_{0.30}Sr_{0.70}Fe_{0.70}Cr_{0.30}O_{3-\delta}$, was also shown to be stable down to a pO_2 of 10^{-20} atm at 800 °C. In a SOFC stack operating on hydrogen fuel, the effective pO_2 depends on the amount of the H_2O reaction product that is present, and it increases along the fuel flow direction as H_2 is consumed and H_2O is produced. The present oxide is at best barely stable under the most reducing condition encountered in a SOFC; for example, $pO_2 \sim 10^{-22}$–10^{-23} atm at 800 °C (corresponding to approximately 97% H_2 and 3% H_2O). Nonetheless, in a button-cell test at 800 °C in 97% H_2/3% H_2O fuel with a current density of 500 mA/cm^2, sufficient additional H_2O was apparently generated to maintain the stability of the $La_{1/3}Sr_{2/3}Fe_{2/3}Cr_{1/3}O_{3-\delta}$ anode.[10] Also, if $La_{0.30}Sr_{0.70}Fe_{0.70}Cr_{0.30}O_{3-\delta}$ is reduced beyond the stability limit, it was shown that reoxidation restores the perovskite and phase separation products to a single phase compound.

Acknowledgment. This paper is dedicated to the memory of J.W.R. We gratefully acknowledge the financial support of the Department of Energy (Grant DE-FG02-99ER14999) and the use of the Central Facilities supported by the MRSEC program of the National Science Foundation (DMR-0576097) at the Materials Research Center of Northwestern University. The neutron diffraction work was performed on the General Purpose Powder Diffractometer (GPPD) at the Intense Pulsed Neutron Source at Argonne National Laboratory. We especially thank the GPPD staff, including Mr. Evan Maxey and Dr. Ryoji Kiyanagi, for experimental assistance and insightful discussions regarding the analysis of powder diffraction data.

Supporting Information Available: XRD patterns of samples with the nominal stoichiometries $La_{0.333}Sr_{0.667}Fe_{0.60}Cr_{0.40}O_{3-\delta}$, $La_{0.333}Sr_{0.667}Fe_{0.50}Cr_{0.50}O_{3-\delta}$, and $La_{0.333}Sr_{0.667}Fe_{0.25}Cr_{0.75}O_{3-\delta}$ (Figure S1), DTA curve of the $La_{0.30}Sr_{0.70}Fe_{0.70}Cr_{0.30}O_{3-\delta}$ and $LaCrO_3$ samples heated at a rate of 5 °C/min in air (Figure S2), and chemical linear expansion of $La_{0.30}Sr_{0.70}Fe_{0.70}Cr_{0.30}O_{3-\delta}$ and corresponding measured partial oxygen pressure plotted versus time at 900 °C (Figure S3). This material is available free of charge via the Internet at http://pubs.acs.org.